





# In vivo localization of iron starvation induced proteins under variable iron supplementation regimes in *Phaeodactylum tricornutum*

Elena Kazamia<sup>1</sup>  | Jan Mach<sup>2</sup> | Jeffrey B. McQuaid<sup>3,4</sup> | Xia Gao<sup>1</sup> | Tyler H. Coale<sup>5</sup> | Ronald Malych<sup>2</sup>  | Jean-Michel Camadro<sup>6</sup>  | Emmanuel Lesuisse<sup>6</sup> | Andrew E. Allen<sup>3,5</sup>  | Chris Bowler<sup>1</sup> | Robert Sutak<sup>2</sup> 

<sup>1</sup>Institut de Biologie de l'ENS (IBENS), Département de Biologie, École Normale Supérieure, CNRS, INSERM, Université PSL, Paris, France

<sup>2</sup>Department of Parasitology, Faculty of Science, Charles University, Vestec, Czech Republic

<sup>3</sup>Microbial and Environmental Genomics, J. Craig Venter Institute, La Jolla, California, USA

<sup>4</sup>The Alfred Wegener Institute, Helmholtz Centre for Polar and Marine Research, Bremerhaven, Germany

<sup>5</sup>Scripps Institution of Oceanography, Integrative Oceanography Division, University of California, San Diego, La Jolla, California, USA

<sup>6</sup>CNRS, Institut Jacques Monod, Université de Paris, Paris, France

## Correspondence

Elena Kazamia, Institut de Biologie de l'ENS (IBENS), Département de Biologie, École Normale Supérieure, CNRS, INSERM, Université PSL, 75005 Paris, France.  
Email: [kazamia@bio.ens.psl.eu](mailto:kazamia@bio.ens.psl.eu)

## Funding information

Marie Curie, Grant/Award Number: H2020; Czech Science Foundation, Grant/Award Number: 07822S; Agence Nationale de la Recherche, Grant/Award Number: CE01-0008; European Research Council; European Union; Horizon 2020; National Science Foundation; Department of Energy; Gordon and Betty Moore Foundation

## Abstract

The model pennate diatom *Phaeodactylum tricornutum* is able to assimilate a range of iron sources. It therefore provides a platform to study different mechanisms of iron processing concomitantly in the same cell. In this study, we follow the localization of three iron starvation induced proteins (ISIPs) in vivo, driven by their native promoters and tagged by fluorophores in an engineered line of *P. tricornutum*. We find that the localization patterns of ISIPs are dynamic and variable depending on the overall iron status of the cell and the source of iron it is exposed to. Notwithstanding, a shared destination of the three ISIPs both under ferric iron and siderophore-bound iron supplementation is a globular compartment in the vicinity of the chloroplast. In a proteomic analysis, we identify that the cell engages endocytosis machinery involved in the vesicular trafficking as a response to siderophore molecules, even when these are not bound to iron. Our results suggest that there may be a direct vesicle traffic connection between the diatom cell membrane and the periplastidial compartment (PPC) that co-opts clathrin-mediated endocytosis and the “cytoplasm to vacuole” (Cvt) pathway, for proteins involved in iron assimilation.

Proteomics data are available via ProteomeXchange with identifier PXD021172.

## Highlight

The marine diatom *P. tricornutum* engages a vesicular network to traffic siderophores and phytotransferrin from the cell membrane directly to a putative iron processing site in the vicinity of the chloroplast.

## KEYWORDS

diatoms, fluorescent proteins, iron, iron starvation induced proteins, *P. tricornutum*, proteome, siderophores

Emmanuel Lesuisse died 12 August 2021

This is an open access article under the terms of the [Creative Commons Attribution-NonCommercial-NoDerivs](https://creativecommons.org/licenses/by-nc-nd/4.0/) License, which permits use and distribution in any medium, provided the original work is properly cited, the use is non-commercial and no modifications or adaptations are made.

© 2022 The Authors. *Plant Direct* published by American Society of Plant Biologists and the Society for Experimental Biology and John Wiley & Sons Ltd.

## 1 | INTRODUCTION

Iron is essential for cellular life. Its flexible redox chemistry confers reactivity to the fundamental metabolic processes of respiration, photosynthesis, and nitrogen fixation. However, the redox flexibility that makes iron desirable for metabolism complicates its chemical speciation in the environment. Both the ionic state and ligand binding of iron depend on the pH and mineral chemistry of its ambient environment. When unicellular life first evolved in the ocean, surface waters were less oxygenated than today, and iron was abundantly present as uncomplexed  $\text{Fe}^{2+}$ . In today's oxygenated ocean, there is significantly less dissolved iron (<2 nM; Boyd & Ellwood, 2010) and this predominantly in its oxidized, ferric form ( $\text{Fe}^{3+}$ ). Of this dissolved pool, the vast majority (an estimated 99%) is organically complexed, and the remaining 1% is labile inorganic iron ( $\text{Fe}^{\prime}$ ) coupled to oxyhydroxides (Gledhill & Buck, 2012). Whether the different chemical forms of iron are bioavailable to marine microorganisms depends on the molecular machinery encoded by individual species. The processing of iron inside cells is subject to careful homeostasis. An excess of iron may be toxic, because of an imbalance of the redox chemistry of the cell and accumulation of reactive oxygen species.

Diatoms are the most successful marine microbial eukaryotes in the contemporary ocean, ubiquitous and abundant, estimated to contribute up to 40% of marine carbon fixation (Granum et al., 2005). Their evolutionary origin involves at least two endosymbiotic events, the first of which occurred 1.5 billion years ago, when a eukaryotic heterotroph assimilated or was invaded by a cyanobacterium, a point in evolutionary history diatoms share with green plants or Viridiplantae. Divergence came an estimated 500 million years later, when a secondary endosymbiosis occurred in which a eukaryotic heterotroph captured a red alga, which subsequently established the Stramenopile lineage to which diatoms belong (Bhattacharya et al., 2004).

It is widely considered that the ecological success of diatoms is in large part because of their iron physiologies, which are highly adapted to the contemporary ocean's iron chemistry (e.g., Marchetti et al., 2012; Morrissey & Bowler, 2012). Open ocean diatoms are able to survive in waters that are chronically iron poor, but often dominate algal blooms induced by iron fertilization, for example, through eolian input (reviewed in Maher et al., 2010). In the field of diatom research, three types of iron physiology adaptations have been proposed: decreased iron requirements, efficient Fe homeostasis and storage, and superior Fe uptake strategies. With respect to decreased iron quotas, functional replacements of ferroproteins with non-iron requiring alternatives have been widely investigated, such as the replacement of ferredoxin with flavodoxin (La Roche et al., 1996), which uses flavin rather than iron as a redox cofactor in the electron carrier, or the substitution of the iron-requiring cytochrome  $c_6$  with the copper-coordinating plastocyanin (Peers & Price, 2006). Nevertheless, such replacements are not ubiquitous among diatom species, and the reconfiguring of cell photosynthesis and carbon storage in response to iron stress is enacted across a wide range of metabolic processes that are often species specific (Groussman et al., 2015; Smith et al., 2016; Caputi et al., 2019).

A portfolio of iron starvation induced proteins (ISIPs) was identified as likely protein candidates for conferring the ability of diatoms to survive periods of prolonged iron deprivation. In early transcriptomic analyses of *P. tricornutum*, a model pennate diatom with a sequenced genome (Bowler et al., 2008), grown under iron replete and iron deplete conditions, transcripts of genes encoding the ISIP1, ISIP2A, and ISIP3 proteins exhibited the highest fold change in response to  $\text{Fe}^{\prime}$  limitation (Allen et al., 2008). Their environmental importance has been verified by comprehensive analysis of the global ocean microbial metacommunity where ISIP transcript abundance was strongly anti-correlated with modeled  $\text{Fe}^{\prime}$  concentrations (Caputi et al., 2019). The roles of the three ISIP proteins remain to be fully elucidated. Thus far, ISIP2A has received the most research attention and was experimentally and phylogenetically shown to be a phyto-transferrin protein, binding dissolved  $\text{Fe}^{3+}$  using pH-sensitive carboxylate functional groups and thus mediating the uptake of  $\text{Fe}^{\prime}$  into the cell (McQuaid et al., 2018; Morrissey et al., 2015). The binding of iron by transferrins is a basal trait, widespread among all domains of life, although the amino acid sequence of diatom ISIP2A has little in common with the canonical transferrin structure.

ISIP1 was shown to be involved in the uptake of siderophore-bound iron via an endocytosis pathway (Kazamia et al., 2018). Mutants deficient in ISIP1 were unable to use siderophore-bound iron, likely because of aborted endocytosis. In the same work, experiments confirmed the cellular destination of the siderophore products to be the chloroplast interior. The phylogenetic origin of ISIP1 appears to be largely diatom specific, although it was also detected in a small subset of pelagophyte and prasinophyte algae (Kazamia et al., 2018). A related protein, p130B identified in *Dunaliella salina*, enabled iron uptake by associating with transferrin on the plasma membrane of cells (Paz et al., 2007). Additionally, it has been suggested that ISIP1 is an iron receptor, based on partial sequence similarity with the low-density lipoprotein receptor LDLR in humans (Lommer et al., 2010). The function of ISIP3 has not been tested physiologically, although bioinformatic annotations predict ferritin-like functional domains (DUF305, PF03713) within conserved sequences (Behnke & LaRoche, 2020).

In the present study, we investigated the localization of three ISIP proteins in vivo in a genetically modified *P. tricornutum* cell line. With each gene driven by its native promoter and coupled to a distinct fluorescent protein (FP), we were able to establish the localization pattern of the three ISIPs in the same cell under conditions of iron stress. We compared this localization pattern with the predicted localization based on state-of-the-art in silico bioinformatic analyses. Next, we identified that the localization of ISIPs is not static and is instead highly dependent on the source of iron that was provided to cells experimentally. Our observations of in vivo ISIP localizations together with published functional studies on these and other proteins suggest a highly nuanced sensing of various iron sources by diatom cells and at least four iron uptake pathways in *P. tricornutum*. Focusing on one of those uptake processes, the assimilation of siderophores, using a proteomic analysis, shed light on putative protein partners to ISIP1. We identify candidate transporter proteins as well as components of



endocytosis machinery likely to be specially adapted to function in diatom cells, which have complicated intracellular compartmentalization, a product of their endosymbiotic origins.

## 2 | MATERIALS AND METHODS

### 2.1 | Culture conditions of *P. tricornutum*

The wild-type (CCMP 2561) and engineered (P611) FP-tagged strain of *P. tricornutum* were grown under a 12-h light/12-h dark cycle, with an average intensity of  $100 \mu\text{mol photons m}^{-2} \text{s}^{-1}$  during the light phase in a Panasonic MLR-352-PE incubator outfitted with Osram Fluora T8 36W fluorescent lamps (with peak illumination at  $\sim 440$  and  $\sim 630$  nm, optimized for plant growth). Cultures were maintained at a temperature of  $18^\circ\text{C}$  at a volume of 20 ml in sterile vented single use polystyrene flasks (Corning). Culture axenicity was confirmed by examining the cultures under the microscope and by standard plating analyses. The growth medium was modified artificial seawater, Mf (Sutak et al., 2010). Its molecular composition is given in Table S1, which also provides a comparison to Aquil media (Morel et al., 1979). The pH was kept at 7.8 throughout growth and during experimental procedures. Reagents, media, and cultures were handled only using plasticware to avoid metal contamination. Where growth is reported, cell counts were taken daily in triplicate using a Malassez chamber.

To starve cultures of iron, cells in mid-exponential phase were collected, separated from growth medium by centrifugation (5000 rpm for 10 min), and triple washed with Mf growth medium spiked with 1 mM EDTA to chelate iron. Cells were resuspended in fresh culture medium with no iron and allowed to grow for a week before the procedure was repeated. Cells that had undergone two rounds of iron starvation and showed a significant decrease in their growth rate compared with wild-type were considered “iron deplete” (denoted as “–Fe” treatments in figures).

### 2.2 | Chemical stocks

Stock solutions of siderophores were prepared as follows: a 10% excess of desferrioxamine solution was added to  $\text{FeCl}_3$  in .1 M HCl to give a 5-mM Fe solution with a Fe:ligand ratio of 1:1.1; after 10 min at room temperature, the pH was adjusted to 7 with 1 M HEPES, and the final 1-mM stock solution was kept at  $20^\circ\text{C}$  until use. The same procedure was followed to obtain siderophore analogs bound to gallium instead of iron. It is important to note that two siderophores were used in our studies, desferrioxamine B (DFB) and desferrichrome (DFCH), which when coupled to iron are noted as ferrioxamine B (FOB) and ferrichrome (FCH), and as Ga-DFCH and Ga-FDB when bound to gallium. The siderophores can be used alternatively, as they both belong to the hydroxamate class of siderophores and are equally bioavailable to *P. tricornutum*, as previously shown by Kazamia et al. (2018). For ferric EDTA (the  $\text{Fe}^{3+}$  source in our experiments), the ligand to iron ratio was 20, and we checked

(by ultracentrifugation) that the complex remained fully soluble during the time of experiments.

All other chemicals including growth medium reagents and batho-phenanthroline disulfonate were purchased from Sigma–Aldrich.

### 2.3 | Generation of trichromatic *P. tricornutum* line P611

To generate the trichromatic *P. tricornutum* line, three independent pUC-19 constructs were built for each ISIP gene by amplifying 600 base-pair promoter + full length gene, fluorescent protein, and 300-bp terminator regions from iron-starved cDNA libraries. Amplifications were performed with Phusion high fidelity polymerase (New England Biolabs) and assembled into pUC-19 using Gibson Assembly cloning. YFP, RFP, and CFP protein tags were used with *ISIP1*, *ISIP2A*, and *ISIP3* genes, respectively; all primer sequences are available in Table S2. Full length constructs were then re-amplified using extra-long primers with 40 base-pair sticky ends—these were complementary to each other as well as the destination cargo plasmid p0521s. p0521s contains a selection marker for bleomycin as well as the URA3 gene flanked by I-SceI sites—this latter marker provides an efficient counter selection to insert DNA sequences using yeast assembly methods (Karas et al., 2015). For assembly, yeast cells were spheroplasted for 20 min prior to adding the three ISIP constructs with the linearized p0521s plasmid (Karas et al., 2015). The final product was assembled in yeast, purified, and re-introduced into *Escherichia coli* containing the conjugation plasmid pRL443 and screened for size with restriction enzymes. Sequence-verified clones were then introduced into *P. tricornutum* by plate mating (conjugation) with *E. coli* for 90 min in the dark at  $30^\circ\text{C}$  as described in Karas et al., 2015. Positive transformants were selected on zeocin antibiotic plates ( $100 \mu\text{g ml}^{-1}$ ) and verified by polymerase chain reaction (PCR) and sequencing. The resulting P611 line was grown in liquid cultures using Mf culture medium supplemented with zeocin ( $100 \mu\text{g ml}^{-1}$ ) during microscopy experiments.

### 2.4 | Confocal microscopy imaging

#### 2.4.1 | Detection of three fluorophores in the line P611

Images were acquired using a confocal imaging microscope, an inverted Leica SP8 (Leica Microsystems, Germany) equipped with 20X/.75 and 63X/1.2 W objectives (HCLP APOC52), a pulsed white light Acousto-Optical Beam Splitter (AOBS) laser, and internal hybrid single-photon counting detectors, HyD SMD 1–4. A water objective was used to minimize light distortion during fluorescence capture, because cells were suspended in the Mf aqueous growth medium. Notch filters were used for each laser, the speed of acquisition was 200 frames per second, with optimized pixel range set to  $3608 \times 3608$ , eight line accumulations, and pixel development time

of 100 ns per frame. Scanning was sequential between frames. Figure S1 shows expected emission and excitation spectra of the FPs.

We optimized image acquisition settings for measuring fluorescence of P611 cells, which were used in all time course experiments. This comprised the following three-step fluorescence acquisition process:

*Sequence 1:* cells were excited by 20  $\mu$ W of 470 nm wavelength, and fluorescence was detected in the window 475–509 nm gated at 1.2 ns. This sequence allowed the measurement of CFP.

*Sequence 2:* cells were excited by a laser pulse at 20  $\mu$ W of 514 nm light, with fluorescence detected in the 519–572 nm range. This sequence measured fluorescence of YFP.

*Sequence 3:* cells were excited at 590 nm (20  $\mu$ W) with fluorescence detected at 595–660 nm as well as at 689–730 nm, the latter using a photomultiplier tube (PMT) detector. The shorter wavelengths detected are indicative of RFP fluorescence, and the PMT detector measured chlorophyll autofluorescence. The signal between RFP and autofluorescence was separated by applying different time gates (0.9–1.7 ns for RFP and 3.6–12.5 ns for autofluorescence). The time gates were established through fluorescence lifetime imaging analysis (Figure S2).

The fluorescence acquisition was done in this order, so that the dimmest fluorophore, CFP, would be detected first, followed by YFP and then the brightest, RFP. Desiccation and bleaching from prolonged laser exposure occurred after approximately 10 min of continuous exposure, such as during a z-stack collection. Images interpreted in this manuscript are from alive cells only.

No FP-associated fluorescence was detected in wild-type cells under these parameters.

## 2.4.2 | Fluorescence lifetime imaging (FLIM)

FLIM images were acquired during confocal imaging on inverted Leica SP8 TCS SMD FLIM (Leica Microsystems, Germany) equipped with 63X/1.2 W objective, a pulsed white light laser (selected excitation wavelength 470 nm, repetition frequency 80 MHz), AOBs, and HyD detectors (measured emission range: 499–601 nm). Single-photon counting signal was detected using the HydraHarp400 module (PicoQuant, Berlin, Germany). FLIM images were processed in SymPhoTime64 software (PicoQuant, Germany). The signals of ISIP2-RFP and chloroplast autofluorescence were separated by Pattern Matching analysis in SymPhoTime software. Pattern matching analysis can separate two populations based on different average lifetime and number of exponential components attributing to decay (Figure S3).

## 2.4.3 | Time courses

For a chosen population of cells, we took 10 images, either every minute between 0 and 10 min, every 10 min over a 0–100 min interval, or in hourly measurements 0–10 h. Ten frames capture was the maximum number of images we could acquire of the cell population

before significant laser damage occurred under our optimized imaging settings. The cells were suspended in their growth medium and placed inside a magnetic cover slip chamber (1 well Chamlide CMS, Quorum Technologies), which decreased the rate of evaporation. The maximum period over which we were able to track a population of cells was 10 h. After that time, cells were desiccated because of culture medium evaporation.

## 2.4.4 | Spectral unmixing

Data for spectral unmixing analysis were acquired on an inverted confocal scanning microscope Carl Zeiss LSM 880 (Carl Zeiss, Germany) equipped with 63X/1.20 W objective, continuous wave lasers, and a spectral 32-channel GaAsP PMT detector. Spectral scans were acquired using 32 channels in the range 410–695 nm; each spectral channel has a width of 9 nm. For the final acquisition, the sample was excited simultaneously with 405, 488, and 561 nm lasers. For reference spectra, CFP was excited by 405 nm laser only, YFP was excited by 488 nm laser only, and RFP was excited by 561 nm only. The spectrum of autofluorescence was selected from the chloroplast region after excitation with a 405 nm laser. However, emission spectra of chloroplast autofluorescence at all the applied excitation wavelengths were identical. Reference emission spectra were obtained by spectral scans of structures labeled with only one fluorescent protein and were used to compile a spectra database (Figure S4A). Spectral scans of samples containing CFP-, YFP- and RFP-labeled ISIP proteins were spectrally decomposed into four components (CFP, YFP, RFP, and autofluorescence) based on saved reference spectra by linear unmixing analysis in ZEN BLACK software (Carl Zeiss, Germany) (Figure S4B).

The spatial resolution of the spectral unmixing method is diffraction limited. Lateral spatial resolution depends on the numerical aperture of the objective (1.2) and the applied excitation and emission wavelengths. Based on the Abbe formula, the achievable lateral resolution in our analysis is  $\sim$ 170 nm for 405 nm excitation,  $\sim$ 200 nm for 488 nm excitation, and  $\sim$ 230 nm for 561 nm excitation (Abbe, 1873).

## 2.5 | Proteomics

### 2.5.1 | Sample preparation for proteomics analyses

For global proteomic analyses, the cells were grown for 1 week in Mf medium containing .1  $\mu$ M iron (as ferric EDTA, Fe<sup>3+</sup>) and then transferred either into iron-deficient Mf medium or into iron-deficient Mf medium containing 1  $\mu$ M Ga (III)-DFCH Ga (III)-DFCH, which is the desferrisiderophore bound to gallium ions. After 3 days, cells from three independent cultures were harvested for each treatment, and cell extracts were prepared by sonication in the presence of .1% digitonin, and the protein content of the samples was measured, in order to quantify the amount of proteins to be precipitated with acetone.



## 2.5.2 | LC-MS/MS acquisition

Protein extracts (40  $\mu\text{g}$ ) were precipitated with acetone at  $-20^{\circ}\text{C}$  (4 v/v sample). The pellet of proteins was collected by centrifugation. The acetone supernatant was carefully removed, and the protein pellet was heated for 20 min at  $95^{\circ}\text{C}$  and then cooled on ice for 20 min. It was resuspended in 20  $\mu\text{l}$  of 25 mM  $\text{NH}_4\text{HCO}_3$  containing sequencing-grade trypsin (12.5  $\mu\text{g ml}^{-1}$ , Promega) and incubated overnight at  $37^{\circ}\text{C}$ . The resulting peptides were desalted using ZipTip  $\mu\text{-C18}$  Pipette Tips (Millipore) and analyzed on a Q-Exactive Plus coupled to a Nano-LC Proxeon 1000 equipped with an Easy Spray ion source (all from Thermo Scientific). Peptides were separated by chromatography with the following parameters: Acclaim PepMap100 C18 pre-column (2 cm, 75  $\mu\text{m}$  i.d., 3  $\mu\text{m}$ , 100  $\text{\AA}$ ), LC EASY-Spray<sup>TM</sup> C18 column (50 cm, 75  $\mu\text{m}$  i.d., 2  $\mu\text{m}$  bead size, 100  $\text{\AA}$  pore size) operated at  $55^{\circ}\text{C}$ , 300 nL/min flow rate, gradient from 95% solvent A (water, .1% formic acid) to 35% solvent B (100% acetonitrile, .1% formic acid) over a period of 97 min, followed by a column regeneration for 23 min, giving a total run time of 2 h. Peptides were analyzed in the Orbitrap cell, in full ion scan mode, at a resolution of 70,000 (at  $m/z$  200), with a mass range of  $m/z$  375–1500 and an Automatic Gain Control (AGC) target of  $3 \times 10^6$ . Fragments were obtained by higher-energy C-trap dissociation (HCD) activation with a collisional energy of 30% and a quadrupole isolation window of 1.4 Da. MS/MS data were acquired in the Orbitrap cell in Top20 mode, at a resolution of 17,500 with an AGC target of  $2 \times 10^5$ , with a dynamic exclusion of 30 s. MS/MS of most intense precursor were acquired first. Peptides with unassigned charge state or singly charged were excluded from the MS/MS acquisition. The maximum ion accumulation times were set to 50 ms for MS acquisition and 45 ms for MS/MS acquisition.

## 2.5.3 | Quantitative analysis in label-free experiments

Label-free quantification in-between subject analysis was performed on raw data with Progenesis-Qi software 4.1 (Nonlinear Dynamics Ltd, Newcastle, UK) using the following procedure: (i) chromatograms alignment, (ii) peptide abundances normalization, (iii) statistical analyses of features, and (iv) peptides identification using the Mascot server through Proteome Discoverer 2.1 (Thermo Scientific). A decoy search was performed and the significance threshold was fixed to .01. The resulting files were imported into Progenesis-LC software. Normalized abundances of proteins from trypsin digests with similar normalized abundance variations of the corresponding peptides (ANOVA  $p$  value  $< .05$ ) were classified together by the AutoClass Bayesian clustering system (Achcar et al., 2009) and visualized with Javavtreeview (<http://jtreeview.sourceforge.net/>).

The mass spectrometry proteomics data have been deposited to the ProteomeXchange Consortium via the PRIDE partner repository (Perez-Riverol et al., 2019) with the dataset identifier PXD021172.

## 3 | RESULTS

### 3.1 | Visualizing the three ISIPs in the same cell

We generated a trichromatic transgenic *P. tricornutum* line we called P611, with ISIP1 tagged to YFP, ISIP2A tagged to RFP, and ISIP3 to CFP. For each protein, the FP tag was C-terminal to the full protein sequence and the construct was driven by native promoters for each gene (see Section 2 for further details). The goal was to observe the patterns of localization for the three proteins in the same cell and compare it to *in silico* targeting predictions.

The *in silico* targeting prediction for the three proteins is the same; in each case, a signal peptide is identified bioinformatically (SignalP 3.0, Bendtsen et al., 2004), which does not have the motif necessary for chloroplast targeting (ASAFind, Gruber et al., 2015), with likely protein destination therefore assigned to the cell endomembrane (Rastogi et al., 2018).

To determine the best time of day to take *in vivo* measurements of fluorescence, we synchronized the cells to a 12-h light/12-h darkness regime and starved them of iron, because this is the condition that promotes *ISIP* expression (Allen et al., 2008). We used the supporting information data to a time-resolved transcriptomic study of *P. tricornutum* under iron limitation (Smith et al., 2016) to anticipate maximum expression and fluorescence levels (Figure S5). *ISIP* expression peaked during darkness and, allowing time for translation, we confirmed maximum fluorescence detection within the first hours after illumination, at the beginning of the light phase.

A typical localization pattern for ISIPs in iron-starved P611 cells imaged as early as possible into the light phase is shown in Figure 1. All three ISIPs localized to the vicinity of the chloroplast midpoint, in a globular region (Figure 1a, d, e), although ISIP2A-RFP showed tighter aggregation at the center of the chloroplast groove (Figure 1e). ISIP1-YFP and ISIP3-CFP co-localize (whether this could be because of a detection error was further investigated). The diameter size of the bright focal point of ISIP2A-RFP was approximately 1.12  $\mu\text{m}$  ( $\text{SD} = .2$ ,  $n = 100$ ), and for ISIP1/ISIP3, it was 3.06  $\mu\text{m}$  ( $\text{SD} = .3$ ,  $n = 100$ ). The average plastid diameter size was 6.21  $\mu\text{m}$  ( $\text{SD} = .5$ ,  $n = 100$ ) measured from differential interference contrast (DIC) images (Figure 1c) rather than autofluorescence, which is variable throughout the day and does not include the chloroplast membranes. The average cell diameter of trichromatic cells was 23.2  $\mu\text{m}$  ( $\text{SD} = 4.0$ ,  $n = 100$ ) and did not deviate significantly from wild-type (*wt* diameter = 23.0  $\mu\text{m}$ ,  $n = 100$ ). In their majority, cells were fusiform, with a small subpopulation of oval cells ( $<1\%$  of the total population). Chlorophyll autofluorescence is shown in Figure 1b, and it was successfully “gated-out” from interfering with FP emission measurements (see Section 2 and Figure S2). Chlorophyll autofluorescence did not interfere with FP detection during experimental procedures.

ISIP1-YFP and ISIP3-CFP showed near perfect co-localization in P611 cells. We performed an additional set of experiments using a Zeiss confocal microscope equipped with 34 detection channels, and a lower, 405-nm excitation wavelength, followed by a procedure of spectral unmixing, to parse emission spectra of YFP from CFP.



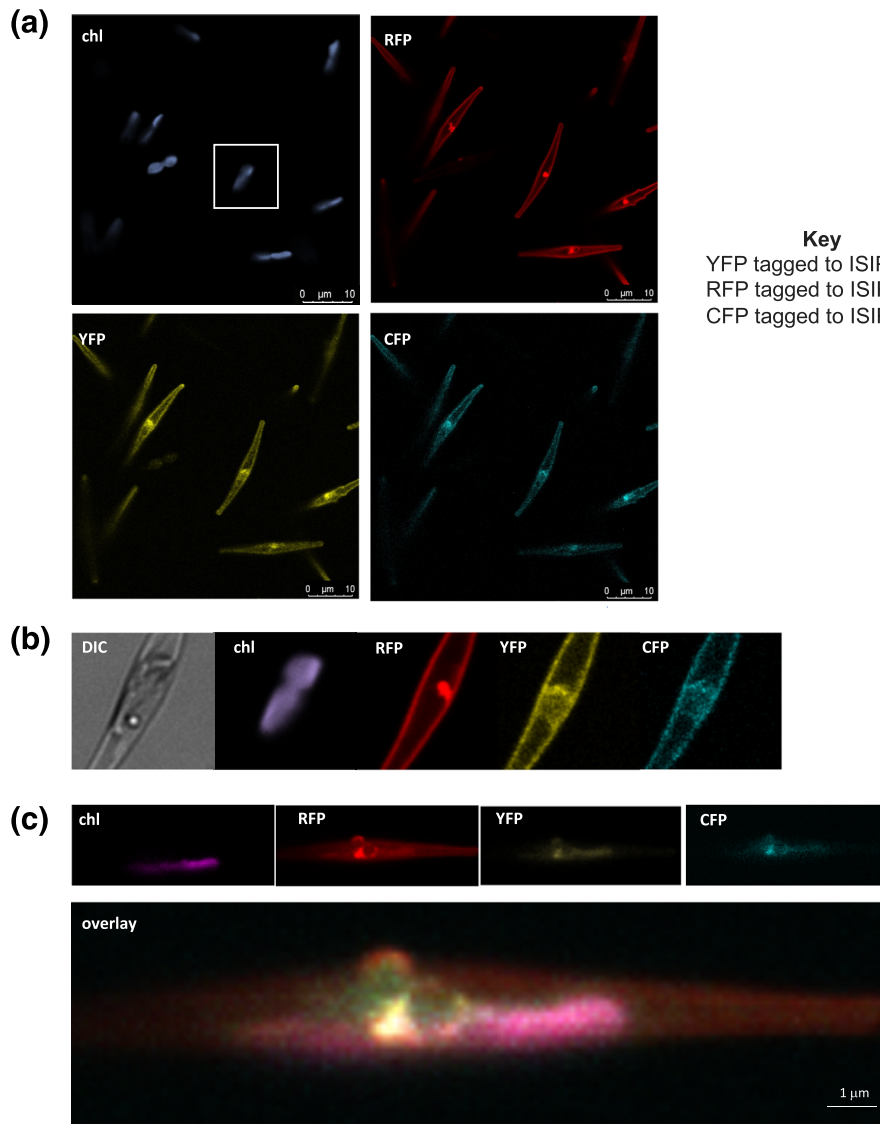


**FIGURE 1** Representative images of Fe-starved *P. tricornutum* P611 trichromatic cell. In this line, ISIP1 is tagged to YFP, ISIP2A to RFP, and ISIP3 to CFP. (a) A field view of P611 cells under the optimized settings on a Leica SP8 confocal microscope (see Section 2). Chlorophyll fluorescence does not interfere with the FPs. (b) Magnified image of the cell region is indicated by the white square in Figure 1 (chl). Differential interference contrast (DIC) is also shown for comparison. YFP and CFP show near perfect co-localization. (c) A representative image of P611 cells captured on the Zeiss confocal microscope using linear unmixing (see Section 2) for comparison

**Key**  
 YFP tagged to ISIP1  
 RFP tagged to ISIP2a  
 CFP tagged to ISIP3

Although we were able to isolate detection of CFP in the cells, its localization under conditions of iron deprivation fully overlapped either one or both of the other fluorophores (Figure S4). It is possible that this is because ISIP3 interacts with these proteins. Further functional analyses are required to test this hypothesis.

### 3.2 | Localization of ISIPs subject to Fe supply

In previous work, we showed that ISIP1 has a dynamic cell localization and can be detected in endocytic vesicles, the chloroplast, and the cell membrane (Kazamia et al., 2018). A similar behavior has also been noted for ISIP2A (McQuaid et al., 2018). To test how ISIP proteins respond dynamically to iron supplementation in vivo, first we conducted time-course experiments with iron pulses. Iron-starved cells were dosed either with Fe' or with the hydroxamate siderophore, ferrioxamine B (FOB) at analogous concentrations. We did not observe significant differences in ISIP localization over a period 0–10 min, 0–1 h, or 0–10 h

(representative 0–10 min time courses shown in supporting information Videos SV1–SV10). Previously, we had quantified that release of siderophore-bound iron delivered via endocytosis to the chloroplast occurs within 4 min of iron addition (Kazamia et al., 2018; supporting information video). Therefore, it is possible that even our fastest time-course analysis (0–10 min) missed this dynamic protein movement, where the first frame is taken after 30 s. It was not possible to take measurements with a faster detection frequency using the available, state-of-the-art microscopy platforms. We conclude that all images we obtained therefore showed cells with a steady state protein localization, which did not change in the first 10 h of iron supplementation.

In addition, we took the approach of pulsing *P. tricornutum* cells with a fluorescently labeled siderophore, a chemical conjugate of FOB with nitrobenzoxadiazole (FOB-NBD). We found that FOB-NBD could recapitulate the observed pattern of localization reported by Kazamia et al. (2018) for wild-type cells, although NBD fluorescence was masked by the stronger YFP signal emerging from the tagged ISIP1 in the P611 line.

Although we were unable to track the same population of cells over a time-course period longer than 10 h because of cell desiccation, we tracked differences in fluorescence in population averages over a period of 5 days following iron supplementation. Based on transcriptomic analyses of the three *ISIPs* (Smith et al., 2016), we expected  $\text{Fe}'$  supplementation to decrease *ISIP1* fluorescence and to have no significant effect on *ISIP2A*-RFP or *ISIP3*-CFP (Figure S5). Intriguingly, we observed that either the addition of siderophore chelated iron (FOB) or labile  $\text{Fe}^{3+}$  ( $\text{Fe}'$ ) both led to a significant decrease in fluorescence of *ISIP1*-YFP and *ISIP2A*-RFP in the cell population, 48 h following supplementation (Figure 2). In that time, there was no overall change in average levels of chlorophyll fluorescence. FOB had the strongest influence, resulting in near complete loss of fluorescence associated with *ISIP1* and *ISIP2A* (Figure 2). Significantly, supplementation of desferrioxamine chelated to gallium instead of iron (+Ga-FDB) had no equivalent effect (Figure 2, fourth row). Instead, the membrane localization of *ISIP1*-YFP under that condition appears

stronger than in iron starved cells, suggesting that the presence of the siderophore induces the movement of *ISIP1*-YFP to the membrane. With  $\text{Fe}'$  supplementation, FP fluorescence disappeared altogether after a further 12 h, that is  $\sim 60$  h from the pulse (data not shown), whereas average chlorophyll autofluorescence remained similar. *ISIP3*-CFP was hardest to image, and it was weakly fluorescent even in iron-starved cells (when fluorescence is expected to be high). We observed a slight increase in fluorescence associated with *ISIP3*-CFP under the Ga-FDB treatment, but this requires further verification.

To revisit the role of reduction in iron uptake at the cell surface of *P. tricornutum* (discussed most recently in Kazamia et al., 2018, McQuaid et al., 2018 and Coale et al., 2019), we additionally supplemented iron-starved *P. tricornutum* cells with  $\text{Fe}'$  in the presence of the  $\text{Fe}^{2+}$  chelator bathophenanthroline disulfonate (BPS) and recorded fluorescence (Figure 2, bottom row). We observed that the localization of *ISIP2A*-RFP in the presence of BPS remained similar to conditions of iron starvation ("no  $\text{Fe}$ " treatment). Our proposed

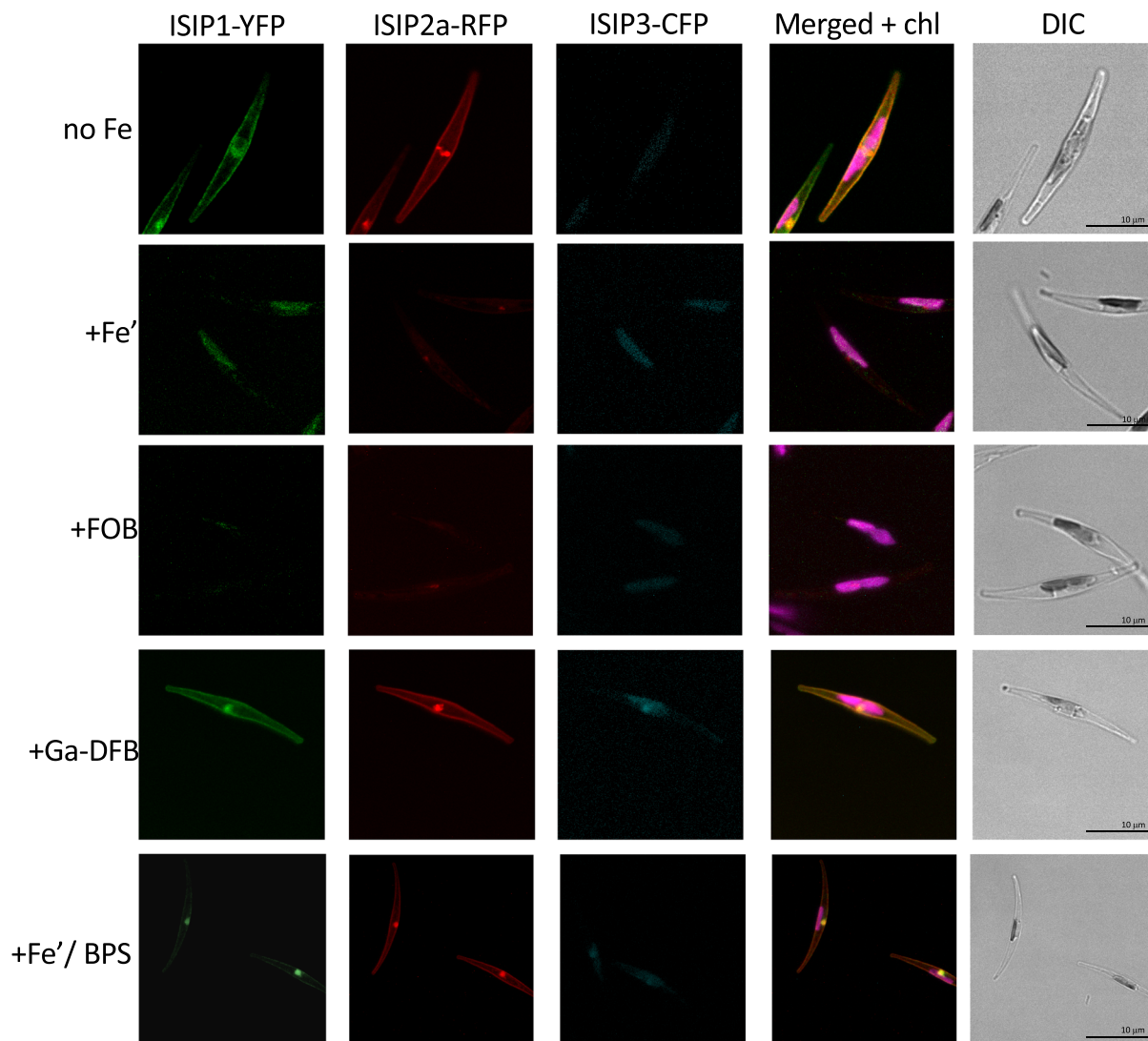


**FIGURE 2** Trichromatic iron-starved line, spiked with a range of iron sources, imaged 48 h after spike. Treatments (top row to bottom): control (no  $\text{Fe}$  spike), labile iron supplemented as iron citrate (1  $\mu\text{M}$ ), siderophore spike (1  $\mu\text{M}$  FOB), gallium analog of siderophore (1  $\mu\text{M}$  Ga-FDB), and  $\text{Fe}'$ /BPS (1  $\mu\text{M}$ /100  $\mu\text{M}$ ) spike to remove  $\text{Fe}^{2+}$  from the cell surface

explanation for the difference between this localization and Fe' supplementation without BPS is that ISIP2A continues to be required and is functional when cells are hindered in reductive iron uptake. In the +Fe' treatment, we are thus observing the global cell response because of reductive Fe' uptake as well as endocytosis mediated by phytotransferrin (ISIP2A) assimilation, which quickly replenishes the iron stocks inside the cell and lowers the requirement of ISIP2A.

Intriguingly, our imaging results suggest that subject to conditions all ISIP proteins at some point in their lifetime converge on a globular compartment in the vicinity of the chloroplast, identifying this region as a possible processing site for iron inside diatom cells. This is visible for ISIP1-YFP and ISIP2A-RFP in "no Fe" treatment and in the "+Ga-FDB" treatment for ISIP3-CFP (Figure 2).

### 3.3 | Summary of iron uptake pathways and likely roles of ISIPs

Overall, our results support the view that there are at least four independent processes of iron assimilation in *P. tricornutum*: direct uptake of ferrous iron at the cell surface (Schallenberg et al., 2015), non-reductive uptake of ferric iron via phytotransferrin (McQuaid et al., 2018; Morrissey et al., 2015), reductive uptake of ferric iron at the cell surface (Lis et al., 2015), and non-reductive uptake of siderophore-bound iron (Coale et al., 2019; Kazamia et al., 2018). Uptake of Fe (II) preceded by reduction of Fe (III) on the cell surface of diatoms has been additionally demonstrated in *Thalassiosira* diatoms (Anderson & Morel, 1980; Shaked et al., 2004). A similar process has also been described in the green alga *Chlamydomonas reinhardtii* (Eckhardt & Buckhout, 1998).

We summarize the role of known proteins in these pathways in Figure 3a. ISIP2A is linked directly to only one of these, whereas ISIP1 is likely to function in two pathways, involved in the assimilation of bound ferric iron either by siderophores or transferrin. The role of ISIP3 remains elusive. Although of the three ISIP proteins it is the most globally abundant (Caputi et al., 2019), it is not highly expressed in *P. tricornutum* (Figure S5), and was the hardest to image, exhibiting fluorescence levels just above detection limits. It is likely that either ISIP3 has a role in iron acquisition not captured by our experimental conditions, or that *P. tricornutum* does not rely heavily on this protein.

It is important to note that the rate and affinity for iron of each type of uptake system is predicted to be dependent on the abundance of the iron source and the ambient pH (Figure 3b). Under low pH, reductive uptake of Fe' is predicted to be significantly lower compared to non-reductive iron uptake. This was evidenced in Kazamia et al. (2018), where growth culture medium was kept at a pH of 7.8 and reductive iron uptake processes were slow, and more thoroughly in a mechanistic investigation into the role of carbonate ions (whose concentrations change with pH) in directing ISIP2A-mediated uptake of ferric irons by McQuaid et al. (2018). That others find the phytotransferrin-mediated uptake to be faster under higher pH (Coale et al., 2019; Morrissey et al., 2015) is not surprising and is in agreement with this synthesis (Figure 3b).

### 3.4 | Proteomics analysis of the response of *P. tricornutum* to iron-free siderophore stimulation

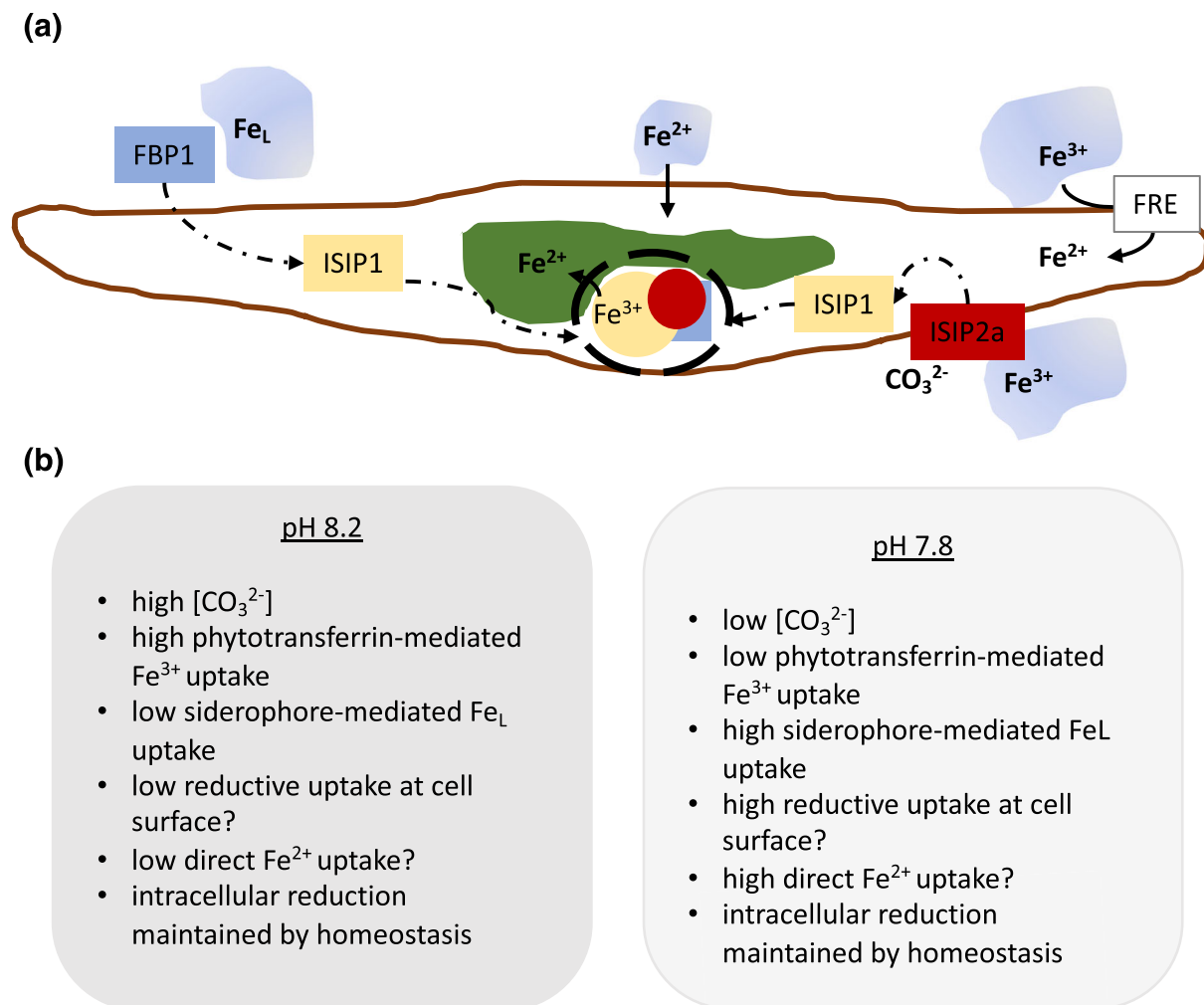
We decided to shed further light on the siderophore uptake pathway by conducting an exploratory proteomics study. Our aim was to compare the protein portfolios of diatom cells that had been pulsed with a siderophore chelated to gallium (Ga-DFCH) with control iron-limited cells (that had not been pulsed with DFCH). In both conditions, the cells were iron starved, which eliminates the confounding factor of the intracellular iron status, which is difficult to measure and control. In the Ga-DFCH treatment, iron starved *P. tricornutum* cells were spiked with the small organic molecule, desferrichrome bound to gallium instead of iron. This comparison allowed us to identify the siderophore response of the cell in the absence of an iron stimulus or change to the overall iron state of the cell. The study was designed to parse out proteins that are involved solely in siderophore uptake, and not in the sensing of iron. We expected the highest concentration of ISIPs under this treatment, based on our microscopy results, which showed the highest fluorescence of all three ISIPs in cells pulsed with a gallium desferrisiderophore (Figure 2).

Table S3 describes the top 100 proteins that showed either an upregulated or repressed response under the two conditions ranked by the *p* values of an analysis of variance (see Section 2 for more details). Of these, one fifth were of unknown function and approximately one third (35/100) were involved in housekeeping cell functions such as cell division. Seven annotated transporter proteins showed a differential response under Ga-DFCH supplementation compared to control treatments. Of these, one transporter protein (NCBI protein ID 219118307), annotated as a "fungal purine transporter," showed the highest fold difference with respect to the proteome from control iron starved cells, albeit with low statistical confidence. It is possible that this transporter is specific to siderophore transport into the cell and is a potential candidate for further study of the siderophore uptake system in diatoms. Both ISIP1 and FBP1 showed significant increases after the addition of the siderophore analog (Figure 4a), as anticipated. Two anion exchange proteins (NCBI IDs 219114320, 441476376) were significantly repressed ( $p < .05$ ) and are both annotated as belonging to the HCO<sub>3</sub><sup>-</sup> transporter family. This suggests that siderophore processing is linked with intricate intracellular pH homeostasis. A paralog of ISIP2A, more similar to Fea1 (NCBI ID 219122261), also showed statistically significant increases compared to controls.

Major changes were detected in putative endocytosis and membrane trafficking pathways of the cell, whose proteins were consistently more abundant in the Ga-DFCH treated cells (Figure 2b). Both clathrin and its major adaptor protein, epsin, showed striking quantitative increases, albeit of low statistical significance, compared to the proteome of control cells, further corroborating the observations that siderophore uptake occurs via endocytosis (Kazamia et al., 2018). Two putative components of exocytosis were repressed with their fold changes shown in Figure 4b.

Finally, 16 proteins linked to micronutrient metabolism showed significant changes in their abundance in iron starved cells stimulated





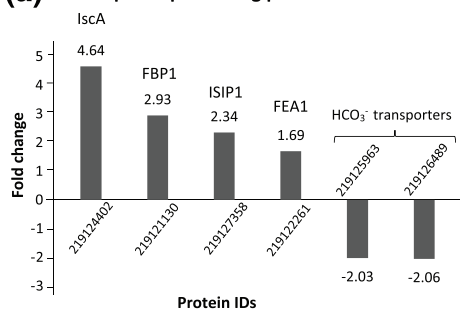
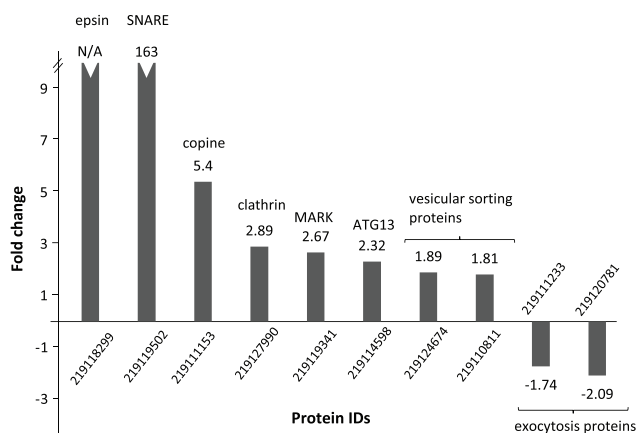
**FIGURE 3** Summary of iron uptake systems in *P. tricornutum*. (a) Synthesis schematic of the known iron uptake and processing mechanisms in *P. tricornutum*. The iron pool is partitioned into three components: ligand bound Fe (Fe<sub>L</sub>), Fe<sup>2+</sup>, and Fe<sup>3+</sup>. Uptake of Fe<sup>2+</sup> has not been measured directly but is presumed to be fast and prevalent in all diatoms. This is the smallest iron pool available, as the majority of iron is either chelated or oxidized. Soluble Fe<sup>3+</sup> (as in an Fe-EDTA system or Fe<sup>3+</sup> supplementation through iron citrate addition) is taken-up either through a phytotransferrin-mediated uptake system or a reductive process on the cell surface (indicated here by FRE). The former is preferred under higher pH when the concentration of dissolved carbonate is lower and phytotransferrin (ISIP2A) is more efficient. Siderophore uptake is via extracellular binding to specialized proteins, including FBP1 and mediated via endocytosis, coordinated by ISIP1. The proposed intracellular dynamics of ISIP1 are shown by arrows and include a possible association with ISIP2A. The ultimate localization of all protein-ligated Fe<sup>3+</sup> (siderophore- and phytotransferrin-bound) is a cite (perhaps a putative organelle, indicated in dashed lines) in the vicinity of the chloroplast (shown in green). This is the site of reduction, by FRE2 in the case of siderophores (Coale et al., 2019), but possibly a wider suite of reductases. (b) Summary of the uptake pathways preferred under low and high pH scenarios, experimentally verified in *P. tricornutum*

with Ga-DFCH. Of these, 13 were induced and are likely involved in siderophore processing. For example, the non-heme iron binding, demethylating protein (NCBI protein ID 219121067) showed a two-fold increase in abundance, as did a putative siderophore synthase (NCBI protein ID 219122041), which may be involved in the breakdown and remodeling of the siderophore molecule (Table S3).

## 4 | DISCUSSION

Understanding how diatoms process iron is an important question in cell physiology that has consequences on global biogeochemistry.

As the contemporary ocean acidifies and warms, the inorganic iron pool is rapidly changing. Geological reconstructions of iron speciation in the ocean indicate that such shifts lead to dramatic changes to photosynthetic life (e.g., Burke et al., 1993), and an understanding of the phytoplankton response is paramount to our predictions of the impacts of climate change. *P. tricornutum* is an excellent model for the study of diatom iron physiology as it appears to harbor the full suite of iron uptake and processing mechanisms that have been described for any diatom (Smith et al., 2016). In this model species, we have the possibility to compare changing iron supplementation regimes on different uptake mechanisms concomitantly in the same cell.

**(a) Siderophore processing proteins****(b) Endocytosis and membrane trafficking proteins**

**FIGURE 4** Proteome comparison of iron limited *P. tricornutum* cells with and without Ga-DFCH supplementation. Iron limited cells (control) compared to cells spiked with Ga-DFCH (treatment). Protein extraction was 3 days after siderophore spike/iron limitation. (a) Putative siderophore or iron processing proteins. (b) Changes to proteins associated with the endocytosis machinery/membrane trafficking of the cell. Further information/annotation is provided in Table S2

The morphology of *P. tricornutum* cells is thoroughly documented, including through electron microscopy imaging (starting with Borowitzka & Volcani, 1978). While there are three morphotypes of *P. tricornutum*, the majority of cells of the model ecotype, which we use here, are fusiform, weakly silicified, and harbor a single plastid, which as in all diatoms is derived from a red algal symbiont (Cavalier-Smith, 2003). The plastid is separated from the rest of the cell by four membranes. The two outermost membranes are the chloroplast endoplasmic reticulum membrane, which is continuous with the host outer nuclear envelope, and the periplastidial membrane. The two innermost membranes correspond to the outer and inner envelope membranes (iEM and oEM, respectively) of the symbiont's chloroplast. Between the periplastidial membrane and the oEM lies a minimized symbiont cytoplasm, the periplastidial compartment (PPC). This space has been described as home to “blob-like structures,” with certain proteins residing in this space permanently (Moog et al., 2011), likely directed here by a modified chloroplast signal peptide (Gruber et al., 2007; Kilian & Kroth, 2005). The cell functions carried out within the PPC remain elusive, because proteins from this compartment have not

been separated from the rest of the cell in the lab. In recent work, a vesicular network was revealed via electron microscopy to exist within the PPC, although canonical components involved in vesicular lipid trafficking were not predicted to be directed here in silico (Flori et al., 2016).

There are three iron starvation induced proteins annotated in diatoms, ISIP1, ISIP2A and ISIP3 (Allen et al., 2008), and we were able to visualize their localization in a trichromatic line of *P. tricornutum*, P611, under a range of scenarios of iron supplementation. It is clear that the localization of the proteins is dynamic; all ISIPs showed an endomembrane localization and a likely PPC localization, which varied depending on the iron supplementation regime. We propose that the aggregation of ISIP proteins we visualize in the PPC of P611 (Figure 3) represents a dedicated iron processing space within this reduced cytoplasm of the secondary endosymbiont. ISIP2A showed a narrower distribution, whereas ISIP1/ISIP3 were slightly more diffuse but directly adjacent. Others have imaged FRE2 and FBP1 tagged with FPs aggregating in an analogous location (Coale et al., 2019). We propose that the confluence of proteins related to iron uptake in this space is to serve as the site of iron reduction, prior to the distribution of ferrous iron as co-factor to the iron-requiring photosynthetic and respiratory machineries. Our hypothesis is that this site is under strict pH regulation, which in turn controls the release of ferrous iron for cell use. It is possible that the bicarbonate transporters identified in the proteomics study we conducted (Table S3 and Figure 4) are involved in the pH regulation of this space. Further physiological experiments are required to test this hypothesis—our work serves merely as a preliminary investigation for further detailed study.

The dynamic localization pattern for ISIP1 and ISIP2A further corroborates the observation that these proteins make use of endocytosis pathways (Kazamia et al., 2018; McQuaid et al., 2018). How the vesicle network operates continuously between the diatom endomembrane and the PPC in diatoms requires further investigation, but because ISIP proteins do not reside in this space permanently, it is not surprising that they lack the PPC-specific targeting motif identified by Gruber et al. (2007). Some of the proteins involved in the endocytosis-mediated uptake of siderophores were identified by our proteomics study. They include canonical clathrin-mediated endocytosis proteins epsin, SNARE, copine, and the microtubule affinity regulating kinase, (MARK) (Figure 4). Intriguingly, our study also picked up a two-fold increase in autophagy-related protein 13, ATG13, during siderophore supplementation. ATG13 is an adaptor protein for the “cytoplasm to vacuole” Cvt pathway originally described in yeast but present in all eukaryotes (Reggiori, Tucker, et al., 2004; Reggiori, Wang, et al., 2004). A major difference between the Cvt pathway and the canonical endocytosis network is that it employs double membrane vesicles and by-passes the Golgi apparatus. Further research is required into the physical connection between the vesicular network identified inside the PPC by Flori et al. (2016) and the cytoplasm/cell membrane of diatoms. Our studies on ISIP proteins suggest, albeit tentatively, that there may be a direct vesicle traffic connection between the diatom cell membrane and the PPC that co-opts clathrin-mediated endocytosis and the Cvt pathway. A unique



proposition that would be apt for diatoms, which have complicated internal structures because of their complex endosymbiotic origins.

We propose that ISIP1 is as an adaptor protein for the vesicular network, engaged to deliver chelated ferric iron bound to proteins to the dedicated iron homeostasis site for processing. In our hands, of the three ISIPs, ISIP1 showed the most dynamic localization, sensitive both to the overall iron status of the cell and the source of iron that the cell is exposed to. In iron replete trichromatic P611 cells, we detected little fluorescence associated with ISIP1-YFP on the cell membrane, which was significantly increased when cells were supplied with siderophores. This is particularly apparent when gallium analogs of the siderophore are used (Figure 2). Supplementation with iron laden siderophores increases membrane fluorescence in the short term, but within 48 h the iron status of the cell changes so total fluorescence is lower, so the effect is easy to miss.

In previous work, we showed experimentally that siderophore uptake and assimilation are inhibited in cells deficient in *ISIP1* (Kazamia et al., 2018). Although knocking down this protein does not impact cell membrane uptake of Fe' via *ISIP2A*, it has not been investigated whether cells deficient in *ISIP1* process intracellular *ISIP2A*-bound ferric iron in the same way as wild-type cells, so an intracellular interaction between *ISIP1* and *ISIP2A* is a likely possibility. A recent study investigating the interactions of *ISIP2A* with other proteins through engineered ascorbate peroxidase APEX2-based subcellular proteomics identifies *ISIP1* as a highly likely interacting partner (Turnšek et al., 2021).

Our study paves the way for further understanding of the localization patterns of three ISIP proteins within the same diatom cell. It was our intention to push in vivo fluorescence imaging in an auto-fluorescent organism to its limits by imaging three FPs in the same cell. We were only able to achieve this complicated process in a single cell line, which serves as a proof of concept. In this study, we demonstrate the technical limits of current state-of-the-art confocal microscopy techniques as applied in vivo to photosynthetic unicellular species. However, our approach clearly has limitations for biological interpretation. Further transgenic lines are required to confirm our initial findings, including analyses of single fluorescent lines. Given availability of resources, it is also advisable to re-sequence any transformants to confirm the desired genetic changes were correctly implemented in the genome without further disruption. Finally, our conclusions regarding the localization of *ISIP3* can use more refinement and testing in other diatom species. The evidence around *ISIP1* and *ISIP2a* studies is more convincing here and in all preceding published literature.

Our study revealed a dynamic pattern of localization of ISIPs in *P. tricornutum* that depends on the source of iron and the overall iron status of the cell. It is likely that siderophore bound and transferrin bound iron is taken for processing to a globular compartment in the vicinity of the chloroplast via a non-canonical endocytosis route, which combines elements of clathrin-mediated and Cvt pathways. Higher-resolution imaging studies are required to confirm this and to clarify whether the destination is the PPC or perhaps even a dedicated iron processing organelle inside the cells, which can be

maintained in careful pH balance, subject to the needs of the mitochondria and the chloroplast for ferrous iron. A caveat is that such studies cannot be currently performed in vivo, until further technological breakthroughs.

## ACKNOWLEDGMENTS

We dedicate this work to the memory of our colleague and friend Emmanuel Lesuisse.

We thank Marie Olsinova and Radek Machan from BIOCEV for their technical help with collecting and analyzing microscopy images, supported by Czech-Biolmaging (LM2018129 and LM2015062) ERDF (CZ.02.1.01/0/0/16\_013/0001775). EK and JMQ were supported by Marie Curie Individual Fellowships H2020 IRONCOMM and IRON-BIND. RS acknowledges the Czech Science Foundation project 18-07822S and CZ.02.1.01/0/0/16\_019/0000759 CePaViP provided by ERDF and MEYS. Funding is acknowledged from the Agence Nationale de la Recherche "Phytomet" (ANR-16-CE01-0008 to CB and EL). CB additionally acknowledges funding from the European Research Council (ERC) under the European Union's Horizon 2020 research and innovation program (Diatomic; grant agreement No. 835067), as well as the French Government "Investissements d'Avenir" programs MEMO LIFE (ANR-10-LABX-54), PSL\* Research University (ANR-11-IDEX-0001-02), and Oceanomics (ANR-11-BTBR-0008). This study was supported by the National Science Foundation Grants NSF-OCE-1756884 and NSF-MCB-1818390 (to A.E.A.); United States Department of Energy Genomics Science program Grant DE-SC0018344 (to A.E.A.); and Gordon and Betty Moore Foundation Grants GBMF3828 and GBMF5006 (to A.E.A.).

## CONFLICTS OF INTEREST

The authors declare no conflict of interest.

## DATA AVAILABILITY STATEMENT

The data generated for this study are available in the Supporting Information. Proteomics data are available via ProteomeXchange with identifier PXD021172.

## ORCID

Elena Kazamia <https://orcid.org/0000-0001-7537-4208>

Ronald Malych <https://orcid.org/0000-0002-7485-2703>

Jean-Michel Camadro <https://orcid.org/0000-0002-8549-2707>

Andrew E. Allen <https://orcid.org/0000-0001-5911-6081>

Robert Sutak <https://orcid.org/0000-0001-5588-1683>

## REFERENCES

- Abbe, E. (1873). Beiträge zur Theorie des Mikroskops und der mikroskopischen Wahrnehmung. *Archiv für Mikroskopische Anatomie*, 9, 413–468. <https://doi.org/10.1007/BF02956173>
- Achcar, F., Camadro, J. M., & Mestivier, D. (2009). AutoClass@ IJM: A powerful tool for Bayesian classification of heterogeneous data in biology. *Nucleic Acids Research* 1;37(suppl\_2):W63-7, 37, W63–W67. <https://doi.org/10.1093/nar/gkp430>
- Allen, A. E., LaRoche, J., Maheswari, U., Lommer, M., Schauer, N., Lopez, P. J., Finazzi, G., Fernie, A. R., & Bowler, C. (2008). Whole-cell response of the pennate diatom *Phaeodactylum tricornutum* to iron

- starvation. *Proceedings of the National Academy of Sciences*, 105(30), 10438–10443. <https://doi.org/10.1073/pnas.0711370105>
- Anderson, M. A., & Morel, F. M. (1980). Uptake of Fe (II) by a diatom in oxic culture medium. *Marine Biology Letters*, 1(5), 263–268.
- Behnke, J., & LaRoche, J. (2020). Starvation-induced proteins (ISIPs). *European Journal of Phycology*, 55(3), 339–360. <https://doi.org/10.1080/09670262.2020.1744039>
- Bendtsen, J. D., Nielsen, H., von Heijne, G., & Brunak, S. (2004). Improved prediction of signal peptides: SignalP 3.0. *Journal of Molecular Biology*, 340(4), 783–795. <https://doi.org/10.1016/j.jmb.2004.05.028>
- Bhattacharya, D., Yoon, H. S., & Hackett, J. D. (2004). Photosynthetic eukaryotes unite: Endosymbiosis connects the dots. *BioEssays*, 26(1), 50–60. <https://doi.org/10.1002/bies.10376>
- Borowitzka, M. A., & Volcani, B. E. (1978). The polymorphic diatom *Phaeodactylum tricornutum*: Ultrastructure of ITS morphotypes. *Journal of Phycology*, 14(1), 10–21. <https://doi.org/10.1111/j.1529-8817.1978.tb00625.x>
- Bowler, C., Allen, A. E., Badger, J. H., Grimwood, J., Jabbari, K., Kuo, A., Maheswari, U., Martens, C., Maumus, F., Otiillar, R. P., & Rayko, E. (2008). The *Phaeodactylum* genome reveals the evolutionary history of diatom genomes. *Nature*, 456(7219), 239–244. <https://doi.org/10.1038/nature07410>
- Boyd, P. W., & Ellwood, M. J. (2010). The biogeochemical cycle of iron in the ocean. *Nature Geoscience*, 3, 675–682. <https://doi.org/10.1038/ngeo964>
- Burke, D. H., Hearst, J. E., & Sidow, A. (1993). Early evolution of photosynthesis: Clues from nitrogenase and chlorophyll iron proteins. *Proceedings of the National Academy of Sciences*, 90(15), 7134–7138. <https://doi.org/10.1073/pnas.90.15.7134>
- Caputi, L., Carradec, Q., Eveillard, D., Kirilovsky, A., Pelletier, E., Pierella Karlusich, J. J., Rocha Jimenez Vieira, F., Villar, E., Chaffron, S., Malviya, S., el Scalco, E., Acinas, S. G., Alberti, A., Aury, J.-M., Benoiston, A.-S., Bertrand, A., Biard, T., Bittner, L., Boccara, M. ... Iudicone, D. (2019). Community-level responses to iron availability in open ocean plankton ecosystems. *Global Biogeochemical Cycles*, 33(3), 391–419. <https://doi.org/10.1029/2018GB006022>
- Cavalier-Smith, T. (2003). Genomic reduction and evolution of novel genetic membranes and protein-targeting machinery in eukaryote-eukaryote chimaeras (meta-algae). *Philosophical Transactions of the Royal Society of London B Biological Sciences*, 358, 109–133. <https://doi.org/10.1098/rstb.2002.1194>
- Coale, T. H., Moosburner, M., Horák, A., Oborník, M., Barbeau, K. A., & Allen, A. E. (2019). Reduction-dependent siderophore assimilation in a model pennate diatom. *Proceedings of the National Academy of Sciences*, 116(47), 23609–23617. <https://doi.org/10.1073/pnas.1907234116>
- Eckhardt, U., & Buckhout, T. J. (1998). Iron assimilation in *Chlamydomonas reinhardtii* involves ferric reduction and is similar to strategy I higher plants. *Journal of Experimental Botany*, 49(324), 1219–1226.
- Flori, S., Jouneau, P. H., Finazzi, G., Maréchal, E., & Falconet, D. (2016). Ultrastructure of the periplastidial compartment of the diatom *Phaeodactylum tricornutum*. *Protist*, 167(3), 254–267. <https://doi.org/10.1016/j.protis.2016.04.001>
- Gledhill, M., & Buck, K. N. (2012). The organic complexation of iron in the marine environment: A review. *Frontiers in Microbiology*, 3, 69.
- Granum, E., Raven, J. A., & Leegood, R. C. (2005). How do marine diatoms fix 10 billion tonnes of inorganic carbon per year? *Canadian Journal of Botany*, 83(7), 898–908. <https://doi.org/10.1139/b05-077>
- Grossman, R. D., Parker, M. S., & Armbrust, E. V. (2015). Diversity and evolutionary history of iron metabolism genes in diatoms. *PLoS ONE*, 10(6), e0129081.
- Gruber, A., Rocap, G., Kroth, P. G., Armbrust, E. V., & Mock, T. (2015). Plastid proteome prediction for diatoms and other algae with secondary plastids of the red lineage. *The Plant Journal*, 81(3), 519–528. <https://doi.org/10.1111/tpj.12734>
- Gruber, A., Vugrinec, S., Hempel, F., Gould, S. B., Maier, U. G., & Kroth, P. G. (2007). Protein targeting into complex diatom plastids: Functional characterisation of a specific targeting motif. *Plant Molecular Biology*, 64, 519–530. <https://doi.org/10.1007/s11103-007-9171-x>
- Karas, B. J., Diner, R. E., Lefebvre, S. C., McQuaid, J., Phillips, A. P. R., Noddings, C. M., Brunson, J. K., Valas, R. E., Deerinck, T. J., Jablanovic, J., & Gillard, J. T. (2015). Designer diatom episomes delivered by bacterial conjugation. *Nature Communications*, 6(1), 1–10, 6925. <https://doi.org/10.1038/ncomms7925>
- Kazamia, E., Sutak, R., Paz-Yepes, J., Dorrell, R. G., Vieira, F. R. J., Mach, J., Morrissey, J., Leon, S., Lam, F., Pelletier, E., Camadro, J. M., Bowler, C., & Lessuisse, E. (2018). Endocytosis-mediated siderophore uptake as a strategy for Fe acquisition in diatoms. *Science Advances*, 4(5), eaar4536.
- Kilian, O., & Kroth, P. G. (2005). Identification and characterization of a new conserved motif within the presequence of proteins targeted into complex diatom plastids. *Plant Journal*, 41, 175–183. <https://doi.org/10.1111/j.1365-3113X.2004.02294.x>
- La Roche, J., Boyd, P. W., McKay, R. M. L., & Geider, R. J. (1996). Flavodoxin as an *in situ* marker for iron stress in phytoplankton. *Nature*, 382, 802–805. <https://doi.org/10.1038/382802a0>
- Lis, H., Shaked, Y., Kranzler, C., Keren, N., & Morel, F. M. (2015). Iron bio-availability to phytoplankton: An empirical approach. *The ISME Journal*, 9(4), 1003–1013. <https://doi.org/10.1038/ismej.2014.199>
- Lommer, M., Roy, A. S., Schilhabel, M., Schreiber, S., Rosenstiel, P., & LaRoche, J. (2010). Recent transfer of an iron-regulated gene from the plastid to the nuclear genome in an oceanic diatom adapted to chronic iron limitation. *BMC Genomics*, 11(1), 718. <https://doi.org/10.1186/1471-2164-11-718>
- Maher, B. A., Prospero, J. M., Mackie, D., Gaiero, D., Hesse, P. P., & Balkanski, Y. (2010). Global connections between aeolian dust, climate and ocean biogeochemistry at the present day and at the last glacial maximum. *Earth-Science Reviews*, 99(1–2), 61–97. <https://doi.org/10.1016/j.earscirev.2009.12.001>
- Marchetti, A., Schrueth, D. M., Durkin, C. A., Parker, M. S., Kodner, R. B., Berthiaume, C. T., Morales, R., Allen, A. E., & Armbrust, V. E. (2012). Comparative metatranscriptomics identifies molecular bases for the physiological responses of phytoplankton to varying iron availability. *Proceedings of the National Academy of Sciences*, 109(6), E317–E325.
- McQuaid, J. B., Kustka, A. B., Oborník, M., Horák, A., McCrow, J. P., Karas, B. J., Zheng, H., Kindeberg, T., Andersson, A. J., Barbeau, K. A., & Allen, A. E. (2018). Carbonate-sensitive phytoferrochelin controls high-affinity iron uptake in diatoms. *Nature*, 555(7697), 534–5377. <https://doi.org/10.1038/nature25982>
- Moog, D., Stork, S., Zauner, S., & Maier, U. G. (2011). *In silico* and *in vivo* investigations of proteins of a minimized eukaryotic cyto-plasm. *Genome Biology and Evolution*, 3, 375–382. <https://doi.org/10.1093/gbe/evr031>
- Morel, F. M., Rueter, J. G., Anderson, D. M., & Guillard, R. R. (1979). Aquil: A chemically defined phytoplankton culture medium for trace metal studies. *Journal of Phycology*, 15(2), 135–141. <https://doi.org/10.1111/j.1529-8817.1979.tb02976.x>
- Morrissey, J., & Bowler, C. (2012). Iron utilization in marine cyanobacteria and eukaryotic algae. *Frontiers in Microbiology*, 3, 43.
- Morrissey, J., Sutak, R., Paz-Yepes, J., Tanaka, A., Moustafa, A., Veluchamy, A., Thomas, Y., Botebol, H., Bouget, F. Y., McQuaid, J. B., Tirichine, L., & Bowler, C. (2015). A novel protein, ubiquitous in marine phytoplankton, concentrates iron at the cell surface and facilitates uptake. *Current Biology*, 25(3), 364–371. <https://doi.org/10.1016/j.cub.2014.12.004>
- Paz, Y., Katz, A., & Pick, U. (2007). A multicopper ferroxidase involved in iron binding to transferrins in *Dunaliella salina* plasma membranes. *Journal of Biological Chemistry*, 282(12), 8658–8666. <https://doi.org/10.1074/jbc.M609756200>





- Peers, G., & Price, N. M. (2006). Copper-containing plastocyanin used for electron transport by an oceanic diatom. *Nature*, 441(7091), 341–344. <https://doi.org/10.1038/nature04630>
- Perez-Riverol, Y., Csordas, A., Bai, J., Bernal-Llinares, M., Hewapathirana, S., Kundu, D. J., Inuganti, A., Griss, J., Mayer, G., Eisenacher, M., Pérez, E., Uszkoreit, J., Pfeuffer, J., Sachsenberg, T., Yilmaz, S., Tiwary, S., Cox, J., Audain, E., Walzer, M., ... Vizcaíno, J. A. (2019). The PRIDE database and related tools and resources in 2019: Improving support for quantification data. *Nucleic Acids Research*, 47(D1), D442–D450. <https://doi.org/10.1093/nar/gky1106>
- Rastogi, A., Maheswari, U., Dorrell, R. G., Vieira, F. R., Maumus, F., Kustka, A., McCarthy, J., Allen, A. E., Kersey, P., Bowler, C., & Tirichine, L. (2018). Integrative analysis of large-scale transcriptome data draws a comprehensive landscape of *Phaeodactylum tricorutum* genome and evolutionary origin of diatoms. *Scientific Reports*, 8(1), 1–4, 4834. <https://doi.org/10.1038/s41598-018-23106-x>
- Reggiori, F., Tucker, K. A., Stromhaug, P. E., & Klionsky, D. J. (2004). The Atg1-Atg13 complex regulates Atg9 and Atg23 retrieval transport from the pre-autophagosomal structure. *Developmental Cell*, 6, 79–90. [https://doi.org/10.1016/S1534-5807\(03\)00402-7](https://doi.org/10.1016/S1534-5807(03)00402-7)
- Reggiori, F., Wang, C. W., Nair, U., Shintani, T., Abeliovich, H., & Klionsky, D. J. (2004). Early stages of the secretory pathway, but not endosomes, are required for Cvt vesicle and autophagosome assembly in *Saccharomyces cerevisiae*. *Molecular Biology of the Cell*, 15, 2189–2204. <https://doi.org/10.1091/mbc.e03-07-0479>
- Schallenberg, C., Davidson, A. B., Simpson, K. G., Miller, L. A., & Cullen, J. T. (2015). Iron (II) variability in the northeast subarctic Pacific Ocean. *Marine Chemistry*, 177, 33–44. <https://doi.org/10.1016/j.marchem.2015.04.004>
- Shaked, Y., Kustka, A. B., Morel, F. M., & Erel, Y. (2004). Simultaneous determination of iron reduction and uptake by phytoplankton. *Limnology and Oceanography: Methods*, 2(5), 137–145.
- Smith, S. R., Gillard, J. T., Kustka, A. B., McCrow, J. P., Badger, J. H., Zheng, H., New, A. M., Dupont, C. L., Obata, T., Fernie, A. R., & Allen, A. E. (2016). Transcriptional orchestration of the global cellular response of a model pennate diatom to diel light cycling under iron limitation. *PLoS Genetics*, 12(12), e1006490. <https://doi.org/10.1371/journal.pgen.1006490>
- Sutak, R., Šlapeta, J., Roman, M. S., Camadro, J. M., & Lesuisse, E. (2010). Nonreductive iron uptake mechanism in the marine alveolate *Chromera velia*. *Plant Physiology*, 154(2010), 991–1000. <https://doi.org/10.1104/pp.110.159947>
- Turnšek, J., Brunson, J. K., Martinez Viedma, M. d. P., Deerinck, T. J., Horák, A., Oborník, M., Bielinski, V. A., & Allen, A. E. (2021). Proximity proteomics in a marine diatom reveals a putative cell surface-to-chloroplast iron trafficking pathway. *eLife*, 10, e52770. <https://doi.org/10.7554/eLife.52770>

## SUPPORTING INFORMATION

Additional supporting information can be found online in the Supporting Information section at the end of this article.

**How to cite this article:** Kazamia, E., Mach, J., McQuaid, J. B., Gao, X., Coale, T. H., Malych, R., Camadro, J.-M., Lesuisse, E., Allen, A. E., Bowler, C., & Sutak, R. (2022). In vivo localization of iron starvation induced proteins under variable iron supplementation regimes in *Phaeodactylum tricorutum*. *Plant Direct*, 6(12), e472. <https://doi.org/10.1002/pld3.472>